Improving Doppler Robustness for Optimized Complementary FM Waveform Subsets

David G. Felton, Jonathan W. Owen, Matthew B. Heintzelman, Daniel B. Herr, Shannon D. Blunt
Radar Systems Lab (RSL), University of Kansas, Lawrence, KS

***Abstract* – In theory, complementary sequences produce no sidelobes in the ideal scenario of zero-Doppler scattering and a distortionless transmitter. Since these conditions are not realistic in practice, a random frequency modulation (RFM) design approach was developed based on the notion of independent complementary subsets, where the FM nature mitigates some of the unavoidable transmitter distortion and subset independence facilitates incoherent sidelobe averaging as a supplement to complementary cancellation.**

While this complementary FM approach previously demonstrated greater resilience compared to theoretical codes (e.g. Golay), it did still only address zero-Doppler. Here, a generalization of that method is developed to enable complementary cancellation over a prescribed Doppler band. Simulation and open-air demonstration of these robust complementary FM waveforms validates that complementary sidelobe cancellation is preserved under Doppler effects.

Keywords–complementary waveforms, noise radar, waveform diversity

I. Introduction

The concept of complementary sequences was initially proposed by Golay in 1949 [1] and later formally defined in 1961 [2] as code pairs with out-of-phase autocorrelation coefficients that sum to zero. However, the connection from mathematical theory to physical experimentation has only recently been made [3,4] due to some practical limitations of complementary codes. The first of these stems from the now well-known sensitivity to Doppler, which causes a mismatch deviation from the cancellation condition [5]. Moreover, codes possess a sinc-shaped spectral roll-off that ultimately leads to significant transmitter distortion, thereby causing further deviation mismatch [6]. While some work has been done to address the Doppler limitation (e.g. [7,8]), contending with transmitter distortion necessitates transitioning to a more physically meaningful signal model than the theoretical code structure. Given its suitability for high-power transmitters, FM is a sensible choice.

In [3,4] the random FM (RFM) concept of nonrepeating, yet physically realizable waveforms was applied in the context of complementary combining. Specifically, the particular signal construction denoted as polyphase-code FM (PCFM) permits the joint optimization of subsets of underlying codes that are mapped into physical FM waveforms, thus achieving constant amplitude (for amplifier saturation) and sufficient spectral containment (by implementation structure and parameter design). The pulse-compressed responses of these waveforms are pre-summed in receive processing to elicit complementary cancellation. Further, because each subset of PCFM-coded waveforms is unique, incoherent sidelobe averaging during slow-time processing provides additional suppression robustness in a manner that is Doppler-agnostic.

We now extend this framework by explicitly accounting for Doppler-shifted scattering so that complementary cancellation can be achieved for larger Doppler shifts. Further, the conditions for proper phase transition within the PCFM structure, $\alpha_n \in \{-\pi, \pi\}$, are now explicitly enforced. Range sidelobe minimization often expands the waveform spectral footprint. To contend with this, an explicit spectral containment constraint is incorporated to remain compliant with FCC regulations [9]. The resulting waveform subsets retain complementary cancellation over the prescribed slow-time Doppler, and are shown in simulation to remain spectrally compact after sidelobe minimization.

II. Waveform Signal Model

Consider a baseband, pulsed FM waveform defined on time support $t \in [0, T]$ having the form

$$s(t) = \exp\{j\phi(t)\} \tag{1}$$

in which $\phi(t)$ is the instantaneous phase function corresponding to instantaneous frequency $f(t) = \frac{1}{2\pi}\frac{\partial\phi(t)}{\partial t}$. More specifically, the first-order PCFM waveform model has instantaneous phase

$$\phi(t;\mathbf{x}) = \int_0^t g(\tau) * \left[\sum\nolimits_{n=1}^{N} \alpha_n \delta\big(\tau - (n-1)T_\mathrm{p}\big)\right] d\tau \,, \tag{2}$$

where $g(t)$ is a shaping filter of time support $\left[0, T_\mathrm{p}\right]$, $\delta(t)$ is the impulse function, and vector $\mathbf{x} = \left[\alpha_1, \ldots, \alpha_N\right]^T$ contains the PCFM instantaneous frequency parameters. The integration stage in (2) can be expressed independent of the PCFM parameters, such that the n^{th} quasi-basis function is

$$b_n(t) = \int_0^t g\big(\tau - (n-1)T_\mathrm{p}\big) d\tau \tag{3}$$

and (2) simplifies to their weighted sum via [11]

$$\phi(t;\mathbf{x}) = \sum\nolimits_{n=1}^{N} \alpha_n b_n(t) \,. \tag{4}$$

Moreover, the shaping filter is commonly chosen to be rectangular, such that (3) yields time-shifted linear ramps as

$$b_n(t) = \begin{cases} 0, & 0 \le t \le (n-1)T_\mathrm{p} \\ \frac{\left(t-(n-1)T_\mathrm{p}\right)}{T_\mathrm{p}}, & (n-1)T_\mathrm{p} \le t \le nT_\mathrm{p} \\ 1, & nT_\mathrm{p} \le t \le NT_\mathrm{p} \end{cases} . \tag{5}$$

This work was supported by the Office of Naval Research under Contract #N00014-23-C-1053. DISTRIBUTION STATEMENT A. Approved for Public Release.

To perform numerical optimization, the PCFM signal model is represented digitally as

$$\mathbf{s} = \exp\{j\mathbf{B}\mathbf{x}\}\,, \tag{6}$$

with matrix $\mathbf{B} \in \mathbb{R}^{M\times N}$ containing a discretized version of $b_n(t)$ in each column and $M = KN$ the length of vector $\mathbf{s}$ for "oversampling" factor K relative to 6-dB bandwidth (akin to LFM swept bandwidth). The time-bandwidth product (TB) of the waveform is approximately equal to N. Additional design freedom can be achieved via "overcoding", in which a factor of L more quasi-basis functions (here more linear ramps) are used, or via "overphasing" which expands the permitted phase-change by a factor of D [10].

Original first-order PCFM waveform model required the values in $\mathbf{x} \in \{-D\pi/L, D\pi/L\}$ [6,10] to prevent excessive phase changes (and thus spectral expansion). Instead, consider the modified PCFM signal model

$$\mathbf{s} = \exp\{j(D\pi/L)\mathbf{B}\cos(\mathbf{x})\} = \exp\{j\mathbf{B}\tilde{\mathbf{x}}\}, \tag{7}$$

where $\tilde{\mathbf{x}} = (D\pi/L)\cos(\mathbf{x})$ achieves this condition without requiring a separate constraint.

III. Waveform Optimization

The waveform's matched filter response (i.e. waveform autocorrelation)

$$r(\tau) = \int_{-\infty}^{\infty} s(t)s^*(t-\tau)dt \tag{8}$$

is the basis for range sidelobe assessment. A useful metric is the generalized integrated sidelobe level (GISL) [12]

$$\text{GISL} = \left(\frac{\int_{\Omega_{\text{SL}}} |r(\tau)|^p\, d\tau}{\int_{\Omega_{\text{ML}}} |r(\tau)|^p\, d\tau}\right)^{\frac{2}{p}} \tag{9}$$

in which Ω_{ML} corresponds to the autocorrelation mainlobe interval and Ω_{SL} otherwise captures the interval of sidelobes. The GISL form therefore subsumes the well-known metrics of integrated sidelobe level (ISL) when $p = 2$ and peak sidelobe level (PSL) as $p \to \infty$.

A. Complementary FM

Leveraging the PCFM signal structure [6] and subsequent gradient optimization [3,4], discretize the z^{th} waveform $\mathbf{s}_z$ parameterized by $\mathbf{x}_z$. Pre-summing the Z waveform autocorrelations therefore yields a composite autocorrelation function in which the mainlobe persists and we wish to suppress the sidelobes to the degree possible by determining $\mathbf{x}_z$ for $z = 0, \ldots, Z-1$.

Begin by defining the zero-appended version of $\mathbf{s}_z$ as

$$\bar{\mathbf{s}}_z = \left[\mathbf{s}_z^T \quad \mathbf{0}_{1\times(M-1)}\right]^T \tag{10}$$

with associated frequency representation

$$\mathbf{s}_{\text{f},z} = \mathbf{A}\bar{\mathbf{s}}_z\,, \tag{11}$$

where $\mathbf{A}$ is a $(2M-1)\times(2M-1)$ discrete Fourier transform (DFT) matrix and $\mathbf{A}^H$ is the inverse DFT. The z^{th} waveform's discretized autocorrelation function is thus

$$\mathbf{r}_z = \mathbf{A}^H\left|\mathbf{s}_{\text{f},z}\right|^2\,, \tag{12}$$

via the Fourier relationship between autocorrelation and power spectral density. The composite autocorrelation is then the combined subset, written as

$$\mathbf{r} = \sum\nolimits_{z=0}^{Z-1} \mathbf{r}_z = \mathbf{R}\mathbf{1}_{Z\times 1} \tag{13}$$

for $\mathbf{R} = [\mathbf{r}_0 \quad \cdots \quad \mathbf{r}_{Z-1}]$ and $\mathbf{1}$ a Z-length vector of ones. To minimize the sidelobes in this composite response, consider the discretized representation of (9) [3]

$$J = \frac{\|\mathbf{w}_{\text{SL}} \odot \mathbf{r}\|_p^2}{\|\mathbf{w}_{\text{ML}} \odot \mathbf{r}\|_p^2} \tag{14}$$

in which $\|\bullet\|_p$ is the p-norm, and $\mathbf{w}_{\text{SL}}$ and $\mathbf{w}_{\text{ML}}$ are binary valued selection vectors corresponding to Ω_{SL} and Ω_{ML} in (9), respectively. Minimization of (14) jointly for the subset of $\mathbf{x}_z$ vectors produces a subset of Z PCFM waveforms.

The discrete and parameterized signal model permits numerical optimization of each waveform subset. The gradient operator with respect to the z^{th} waveform parameters $\mathbf{x}_z$ for $z = 0, \ldots, Z-1$ is

$$\nabla_{\mathbf{x}_z} = \left[\frac{\partial}{\partial\alpha_{1,z}} \quad \cdots \quad \frac{\partial}{\partial\alpha_{N,z}}\right]^T. \tag{15}$$

Applying this gradient to (14) then yields [3]

$$\begin{aligned}\nabla_{\tilde{\mathbf{x}}_z} J = 4J\overline{\mathbf{B}}^T\Im\Bigg\{\bar{\mathbf{s}}_z^* \odot \mathbf{A}^H\Bigg[\mathbf{s}_{\text{f},z} \odot \\ \mathbf{A}\left(\left[\frac{\mathbf{w}_{\text{SL}}}{\|\mathbf{w}_{\text{SL}}\odot\mathbf{r}\|_p^p} - \frac{\mathbf{w}_{\text{ML}}}{\|\mathbf{w}_{\text{ML}}\odot\mathbf{r}\|_p^p}\right] \odot |\mathbf{r}|^{p-2} \odot \mathbf{r}\right)\Bigg]\Bigg\}\end{aligned} \tag{16}$$

where

$$\overline{\mathbf{B}} = \left[\mathbf{B}^T \quad \mathbf{0}_{N\times M-1}\right]^T \tag{17}$$

to align dimensionalities with (10). Here $\Im\{\cdot\}$ extracts the imaginary part of the argument and $\mathbf{0}$ is a zeros matrix. Since (14) is highly non-convex, the values in the Z vectors $\mathbf{x}_z$ are updated iteratively to reach the local minima (uniqueness across independently initialized subsets is achieved by this non-convexity). Note that relative to [3] the gradient must be altered to reflect the inclusion of (7), which results in

$$\nabla_{\mathbf{x}_z} = -(D\pi/\text{L})\sin(\mathbf{x}_z) \odot \nabla_{\tilde{\mathbf{x}}_z}\,. \tag{18}$$

The iterative update of the z^{th} waveform's parameters is thus

$$\mathbf{x}_{z,i+1} = \mathbf{x}_{z,i} + \mu_{z,i}\mathbf{p}_{z,i}\,, \tag{19}$$

where $\mathbf{p}_{z,i}$ is a descent direction for the z^{th} waveform at the i^{th} iteration, and $\mu_{z,i}$ is the step size selected such that $\mathbf{x}_{z,i+1}$ is ensured to reduce (14) via a line search along direction $\mathbf{p}_{z,i}$. The choice of step size and direction involves a balance between computational complexity and convergence speed [14].

B. Doppler-Generalized (DG) Complementary FM

The sidelobe suppression of complementary codes is known to degrade significantly in the presence of slow-time Doppler. In [3], complementary FM waveforms were shown to degrade more gracefully. Here we take that robustness a step further.

Generalize (13) to account for Doppler via

$$\mathbf{r}_\omega = \sum_{z=0}^{Z-1} \mathbf{r}_z e^{jz\omega} = \mathbf{R}\mathbf{u} \tag{20}$$

for $\omega \in \{-\pi/Z, \pi/Z\}$ representing the normalized Doppler space after pre-summing on receive. Then concatenate the collection of complementary responses for a discretization into U unique normalized Doppler frequencies as

$$\mathbf{R}_\Omega = \mathbf{R}\mathbf{U} = [\mathbf{r}_{\omega_0} \quad \cdots \quad \mathbf{r}_{\omega_{U-1}}] \,. \tag{21}$$

Consequently, an altered version of (14) that collectively captures the Z waveforms and U Dopplers can be written as

$$J_\Omega = \frac{\|\mathbf{W}_{\text{SL}} \odot \mathbf{R}_\Omega\|_p^2}{\|\mathbf{W}_{\text{ML}} \odot \mathbf{R}_\Omega\|_p^2} \tag{22}$$

for $\|\bullet\|_p$ now an element-wise matrix p-norm and

$$\mathbf{W}_{\text{SL}} = \mathbf{w}_{\text{SL}}\mathbf{1}_{U\times 1}^T; \;\; \mathbf{W}_{\text{ML}} = \mathbf{w}_{\text{ML}}\mathbf{1}_{U\times 1}^T \tag{23}$$

to expand the selection vectors to match the dimensionality of (21). The gradient of (22) then becomes

$$\nabla_{\tilde{\mathbf{x}}_z} J_\Omega = 4J_\Omega \overline{\mathbf{B}}^T \Im\left\{\bar{\mathbf{s}}_z^* \odot \mathbf{A}^H \left[\mathbf{s}_{\text{f},z} \odot \Re\left\{\mathbf{A}\left(\left[\frac{\mathbf{W}_{\text{SL}}}{\|\mathbf{W}_{\text{SL}} \odot \mathbf{R}_\Omega\|_p^p} - \frac{\mathbf{W}_{\text{ML}}}{\|\mathbf{W}_{\text{ML}} \odot \mathbf{R}_\Omega\|_p^p}\right] \odot |\mathbf{R}_\Omega|^{p-2} \odot \mathbf{R}_\Omega\right) e^{-j\boldsymbol{\omega} z}\right\}\right]\right\} \tag{24}$$

for $\boldsymbol{\omega}$ a $U \times 1$ vector of normalized Doppler values and with $\Re\{\cdot\}$ extracting the real part of the argument. When $U = 1$, the DG complementary FM design is identical to that in (14). Selecting values in $\boldsymbol{\omega}$ that align with expected (or determined) Doppler shifts within an illuminated scene therefore represents a generalization of complementary operation.

C. Augmented Lagrangian

It is known that a Gaussian spectral density has a Fourier relationship with a Gaussian autocorrelation, where the latter achieves extremely low sidelobes in practice [13]. However, this spectral density has a somewhat gradual roll-off that necessitates a high degree of "over-sampling" for optimization and receive processing, which may be undesirable (note this roll-off is still far more contained than the sinc roll-off of phase codes). Since optimization to suppress sidelobes can tend toward this Gaussian condition, it can be useful to impose a spectral containment constraint.

The selection of $\mathbf{w}_{\text{ML}}$ provides an implicit degree of spectral containment because the mainlobe width is inversely proportional to the signal bandwidth [16,17]. Also consider the explicit spectral constraint

$$\left\| \mathbf{w}_{\text{f}} \odot \frac{1}{Z} \sum_{z=0}^{Z-1} \left|\mathbf{s}_{\text{f},z}\right|^2 \right\|_2^2 = \gamma \tag{25}$$

for $\mathbf{w}_{\text{f}}$ a binary-valued spectrum selection vector with ones in the stopband and zeros in the passband. The parameter $\gamma \in [0,1]$ represents a normalized stopband energy which acts as a permittable limit for that region. Now define a constraint function to represent the difference between the energy in $\mathbf{w}_{\text{f}}$ and γ via

$$g = \left\| \mathbf{w}_{\text{f}} \odot \frac{1}{Z} \sum_{z=0}^{Z-1} \left|\mathbf{s}_{\text{f},z}\right|^2 \right\|_2^2 - \gamma \tag{26}$$

with the constraint satisfied when $g < 0$.

To enforce this inequality spectral constraint, the augmented Lagrangian function [15] is posed as

$$\mathcal{L} = J + (\lambda + \frac{\mu}{2} g) g^+ \tag{27}$$

for λ the Lagrange multiplier and μ a penalty parameter that takes on a large value when the constraint is not satisfied. The function $(\bullet)^+ = \max\{0, \bullet\}$ extracts the positive part of the argument, and results such that iff $g > 0$, the penalty parameter μ increases to subsequently place more emphasis on addressing the constraint violation. The resulting gradient of (27) is

$$\nabla_{\mathbf{x}_z} \mathcal{L} = \nabla_{\mathbf{x}_z} J + (\lambda + \mu g)^+ \nabla_{\mathbf{x}_z} g \tag{28}$$

where

$$\nabla_{\tilde{\mathbf{x}}_z} g = 4\overline{\mathbf{B}}^T \Im\left\{\bar{\mathbf{s}}_z^* \odot \mathbf{A}^H \left(\mathbf{w}_{\text{f}} \odot \mathbf{s}_{\text{f},z}\right)\right\} \,. \tag{29}$$

Minimization within this Lagrangian gradient descent framework serves to produce DG complementary FM waveforms with prescribed spectral containment.

IV. Simulation of Comp-FM and DG-Comp-FM

A collection of Q=250 subsets of Z=4 complementary waveforms (total of C=1000 waveforms) were optimized using the approaches above. Both RFM and LFM initializations were considered for a 6-dB bandwidth of 50 MHz and pulse width of 1.28μs (TB=64). The PCFM structure of (7) was parameterized with N=128 terms (L=2 overcoding, D=2 overphasing). Each waveform was oversampled by K=4 so that the discretized waveform length was M=256. Each waveform subset was optimized using "*minf_lbfgs*," a quasi-Newton iterative descent method in the Tensorlab toolbox [18,19] within an Augmented Lagrangian optimization wrapper. The Lagrange multiplier λ and penalty parameter μ were updated 10 times per subset throughout the optimization process to maintain the spectral constraint. Each subset was optimized for $p = 6$ to tend toward a PSL-like solution (i.e. flat) in the regions designated by $\mathbf{w}_{\text{SL}}$.

First consider the optimized waveforms resulting from LFM initialization. To provide some diversity, each initial LFM was perturbed by a small ($\sim 10^{-5}$) random time varying phase to help the subsets reach unique local minima. The resulting coherent and RMS autocorrelations (after complementary combining) are shown in Fig. 1. The perturbed LFM initializations are shown in black, where there is no benefit to pre-summing since the waveform is repeated. Optimizing according to (14) yields the responses in blue, where there is around 91 dB of complementary sidelobe cancellation (CSC) via the 4-waveform subsets along with an additional $10\log_{10}(250) = 24$ dB of incoherent sidelobe cancellation (ISC) due to the independent subsets. In contrast, optimizing according to (24) for the entire effective Doppler interval ($\boldsymbol{\omega} \in \{0, \pi/Z\}$ after pre-summing) yields the results in orange, achieving roughly 48 dB of CSC and the same 24 dB of ISC, a great improvement over LFM but giving up 43 dB relative to the original complementary FM as a trade for broader Doppler utility.

The RFM initialization was accomplished by least-squares mapping from pseudo-random optimized waveforms [20] based on a super-Gaussian template with shaping parameter of 7 [21],

thereby providing a spectrum commensurate with LFM yet with greater randomized time/frequency characteristics. Now the initial waveforms do benefit from ISC because they are random (per Fig. 2). Of course, the quasi-rectangular spectral template does correspond to near-in shoulder lobes. Subset-wise complementary optimization yields an RMS improvement of around 66 dB in PSL, while the Doppler generalized form only achieves about 33 dB PSL improvement in exchange for expanded Doppler utility.

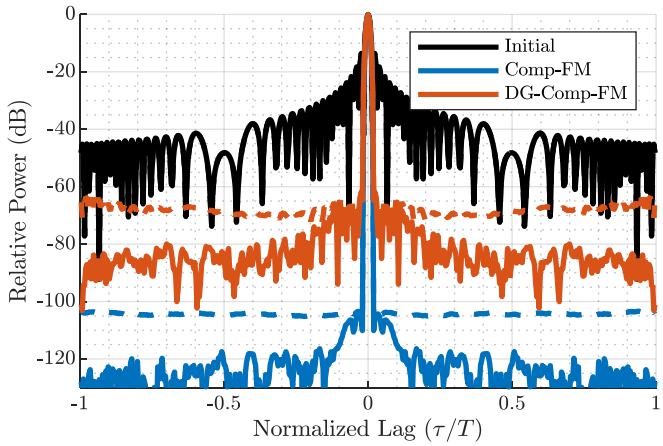

Fig. 1. Coherent (solid) and RMS (dashed) composite autocorrelation of C=1000 waveforms after pre-summing by Z=4 (LFM Initialization)

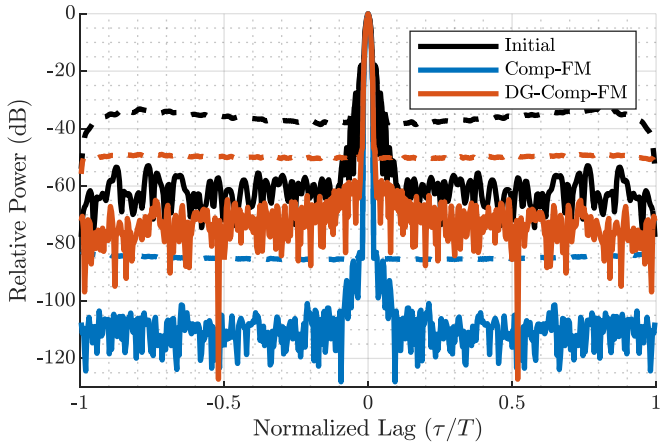

Fig. 2. Coherent (solid) and RMS (dashed) composite autocorrelation of C=1000 waveforms after pre-summing by Z=4 (RFM Initialization)

Of course, Figs. 1 and 2 do not tell the whole story from the perspective of generalizing over Doppler. In Fig. 3 we observe that the DG complementary FM gradient from (24) realizes a nearly flat response across much of the Doppler interval. Compare this result to the original complementary FM approach that provides excellent cancellation at zero-Doppler but exceeds the new approach for normalized Doppler of 0.05. Moreover, the LFM initialization is found to provide markedly better Doppler robustness relative to the RFM initialization (about 15 dB).

Figs. 4 and 5 show the mean power spectra of the different optimization approaches for perturbed LFM and RFM, respectively. Each initialization results in an optimized waveform subset with an aggregate power spectrum approaching a Gaussian, which is more apparent in the passband. In either case, complementary FM subsets result in an aggregate PSD with a very smooth passband (indicating a nearly perfect match to a Gaussian shape), while DG complementary FM subsets instead focus design degrees of freedom to maintain Doppler robustness.

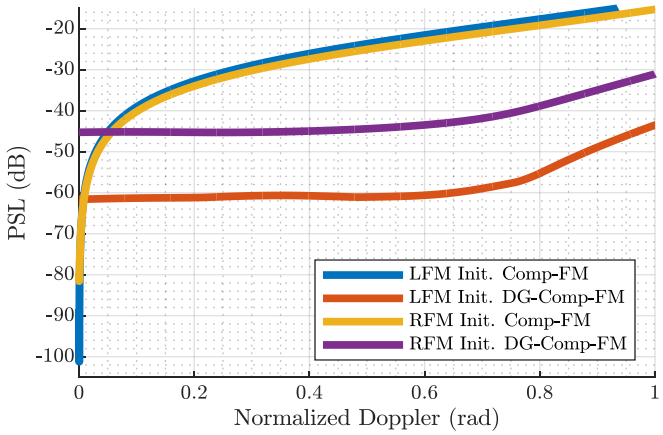

Fig. 3. Mean PSL (across the Q=250 subsets) of composite autocorrelations vs. normalized Doppler

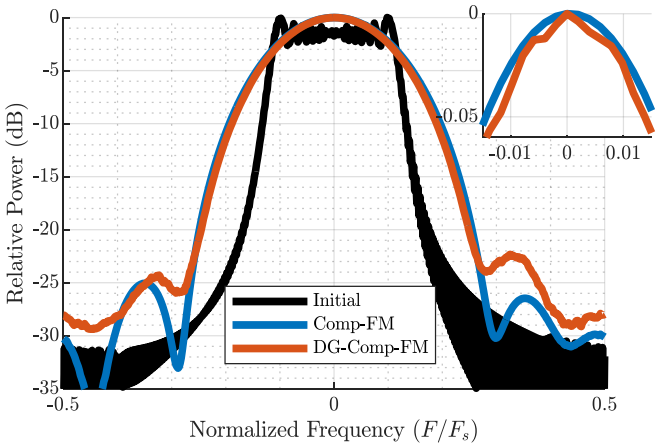

Fig. 4. The mean PSD of (individual) initial perturbed LFM waveforms, and the PSD of waveforms after optimization of (14) and (22)

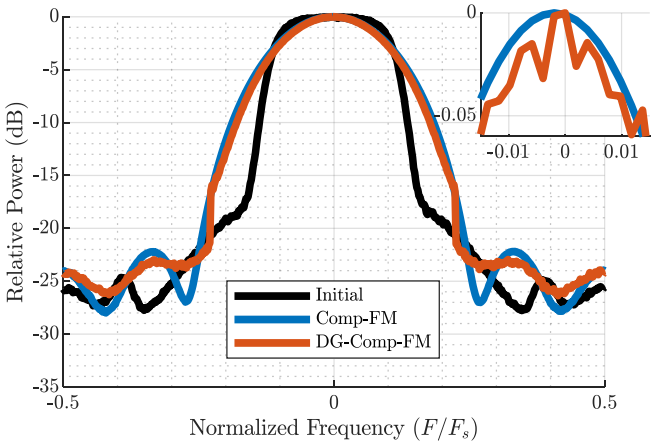

Fig. 5. The mean PSD of (individual) initial RFM waveforms, and the PSD of waveforms after optimization of (14) and (22)

V. Experimental Results

The same C=1000 waveforms were transmitted in an open-air environment, at a center frequency of 3.4 GHz and at a PRF of 8 kHz, which is reduced by a factor of Z=4 to an effective PRF of 2 kHz after pre-summing. The pulses are match filtered in range followed by pre-summing, and a –40 dB Taylor window is applied across slow-time prior to Doppler processing. Each set of waveforms is concatenated into a single coherent processing interval (CPI) so that the observed scene is nearly identical from case to case.

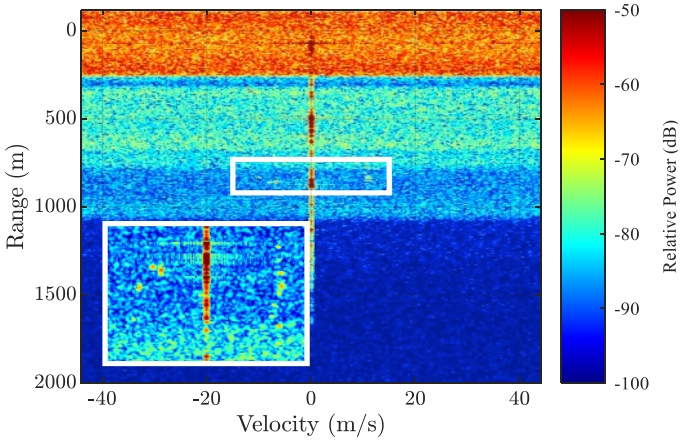

Fig. 6. Open-air range-Doppler response for initial RFM waveforms

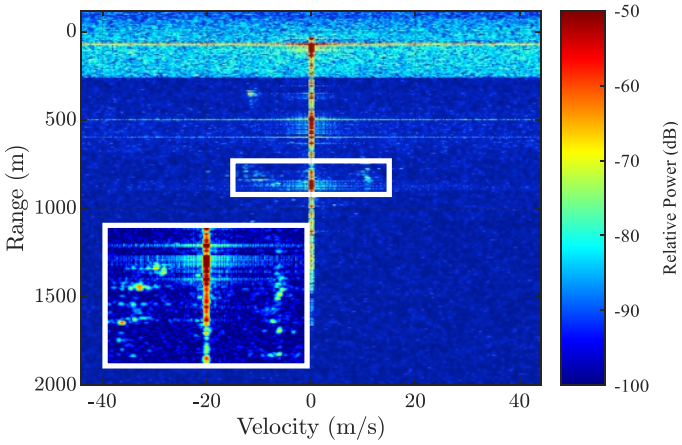

Fig. 7. Open-air range-Doppler response for RFM-initialized complementary FM waveforms

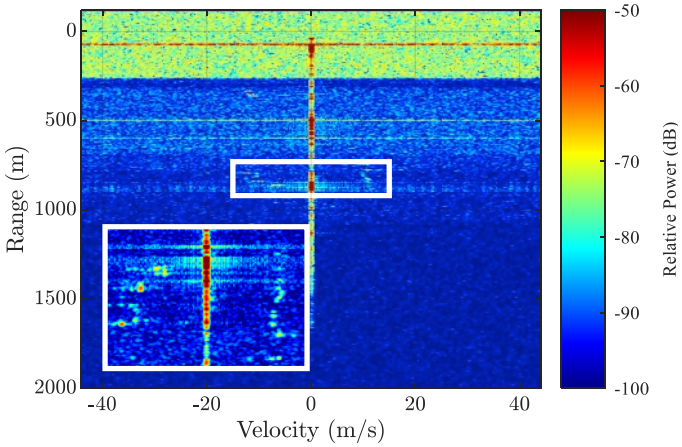

Fig. 8. Open-air range-Doppler response for RFM-initialized DG complementary FM waveforms

The range-Doppler map in Fig. 6 results from the initial sets of RFM waveforms, which acts as a baseline for the optimized subsets. Due to the CPI being pulse-agile, the unique range sidelobes resulting from the high-power direct-path clutter spreads along the Doppler axis, an effect known as range-sidelobe modulation (RSM) [22]. When the optimized complementary FM subsets (initialized by RFM) are pre-summed, the direct path RSM is greatly reduced in Fig. 7, which uncovers otherwise obfuscated movers. Likewise, in Fig. 8 DG complementary FM reduces direct path RSM, though to a lesser degree relative to complementary FM because degrees of freedom are allocated over a larger Doppler space.

While there are movers in the scene, their range-Doppler sidelobes fall below the noise-limited dynamic range and thus do not demonstrate the Doppler induced degradation associated with complementary FM. For the sake of demonstration, an artificial Doppler shift is applied (akin to a moving platform) to shift the direct path clutter to a non-zero Doppler to show the degradation of complementary FM. Of course, moving platforms also invoke Doppler bandwidth along the clutter ridge that would degrade complementarity, which cannot be corrected with a simple transformation.

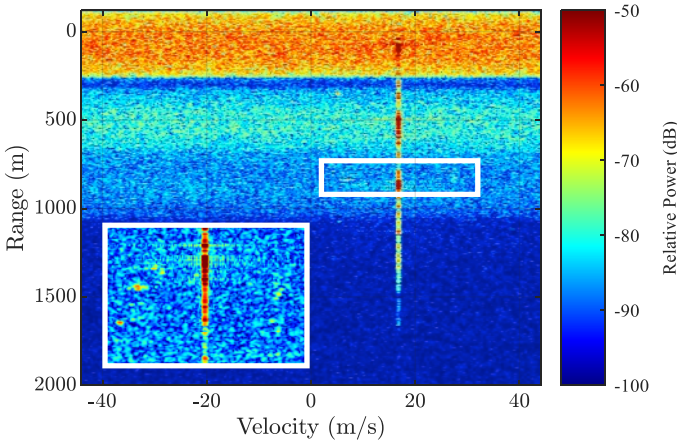

Fig. 9. Open-air range-Doppler response for RFM-initialized complementary FM waveforms, with artificial Doppler shift

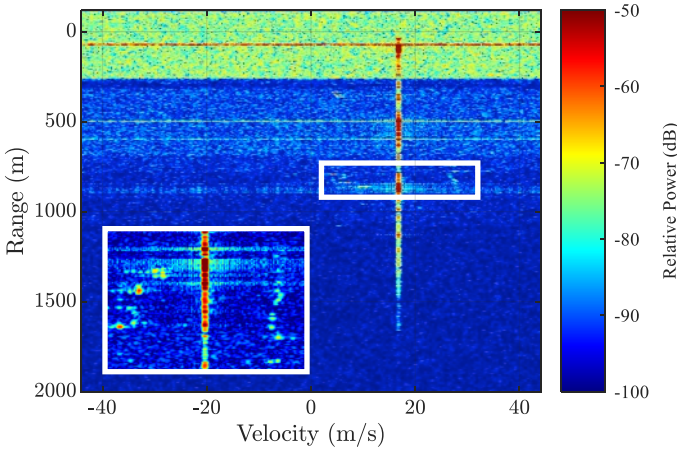

Fig. 10. Open-air range-Doppler response for RFM-initialized DG complementary FM waveforms, with artificial Doppler shift.

In Fig. 9 we see that the complementary sidelobe cancellation has degraded as anticipated relative to Fig. 3, to a level nearly identical to Fig. 6. Alternatively, Fig. 10 demonstrates that DG complementary FM fares well despite a significant Doppler shift, resulting in a range-Doppler map almost identical to that in Fig. 8.

VI. Conclusions

Complementary FM has been generalized to achieve robust sidelobe cancellation in the presence of large Doppler. The resulting composite autocorrelation of each subset of PCFM waveforms maintains modest sidelobe cancellation for very low Dopplers (relative to standard complementary FM) which is preserved in the presence of slow-time Doppler shifts. Simulated analysis shows that complementary sidelobe cancellation is possible across the entire Doppler spectrum within the effective (pre-summed) Doppler interval. Open air demonstration further validates that Doppler generalized complementary FM waveforms remain transmitter-amenable and retain sidelobe cancellation despite Doppler effects.

REFERENCES

[1] M. J. E. Golay, "Notes on digital coding", *Proc. IEEE*, vol. 37 (1949) p. 657.

[2] M. J. E. Golay, "Complementary series". *IEEE Trans. Inform. Theory*. 7(2), 82–87 (1961).

[3] C.A. Mohr, P.M. McCormick, S.D. Blunt, "Optimized complementary waveform subsets within an FM noise radar CPI," *IEEE Radar Conf.*, Oklahoma City, OK, Apr. 2018.

[4] C.C. Jones, C.A. Mohr, P.M. McCormick, S.D. Blunt, "Complementary frequency modulated radar waveforms and optimised receive processing". *IET Radar Sonar Navig*, 15: 708-723, July 2021.

[5] N. Levanon, I. Cohen, P. Itkin, "Complementary pair radar waveforms evaluating and mitigating some drawbacks," *IEEE Aerospace & Electronic Systems Mag*., vol. 32, no. 3, pp. 40-50, Mar. 2017.

[6] S.D. Blunt, M. Cook, J. Jakabosky, J. De Graaf, E. Perrins, "Polyphase-coded FM (PCFM) radar waveforms, part I: implementation," *IEEE Trans. Aerospace & Electronic Systems*, vol. 50, no. 3, pp. 2218-2229, July 2014.

[7] A. Pezeshki, A.R. Calderbank, W. Moran, S.D. Howard, "Doppler resilient Golay complementary waveforms," *IEEE Trans. Information Theory*, vol. 54, no. 9, pp. 4254-4266, Sept. 2008.

[8] W. Dang, A. Pezeshki, S. Howard, W. Moran, R. Calderbank, "Coordinating complementary waveforms for sidelobe suppression," *Asilomar Conf. on Signals, Systems & Computers*, Pacific Grove, CA, Nov. 2011.

[9] Title 47 (Telecommunication), Chapter I (Federal Communications Commission) Subchapter A, Part 15 (Radio Frequency Devices), Electronic Code of Federal Regulations (ECFR) for the United States, Mar. 2024.

[10] J. Jakabosky, S.D. Blunt, B. Himed, "Optimization of "over-coded" radar waveforms," *IEEE Radar Conference*, Cincinnati, OH, May 2014.

[11] B. White, M.B. Heintzelman, S.D. Blunt, "Alternative "bases" for gradient-based optimization of parameterized FM radar waveforms," *IEEE Radar Conf.*, San Antonio, TX, May 2023.

[12] P.M. McCormick, S.D. Blunt, "Nonlinear conjugate gradient optimization of polyphase-coded FM radar waveforms," *IEEE Radar Conf.*, Seattle, WA, May 2017.

[13] C.A. Mohr, P.M. McCormick, C.A. Topliff, S.D. Blunt, J.M. Baden, "Gradient-based optimization of PCFM radar waveforms," *IEEE Trans. Aerospace & Electronic Systems*, vol. 57, no. 2, pp. 935-956, Apr. 2021.

[14] W.W. Hager, H. Zhang, "A survey of nonlinear conjugate gradient methods," *Pacific Journal of Optimization*, vol. 2, no. 1, pp. 35-58, Dec. 2005.

[15] J. Nocedal, S. Wright, *Numerical Optimization*. Springer Science & Business Media, 2006.

[16] J.W. Owen, P.M. McCormick, C.C. Jones, S.D. Blunt, "On the optimality of spectrally notched radar waveform & filter designs," *IEEE Radar Conf.*, San Antonio, TX, May 2023.

[17] L. Cohen, *Time-Frequency Analysis*, ser. Electrical engineering signal processing. Prentice Hall PTR, 1995.

[18] D.C. Liu, J. Nocedal, "On the limited memory BFGS method for large scale optimization," *Mathematical Programming*, vol. 45, pp. 503–528, Aug. 1989.

[19] N. Vervliet, O. Debals, L. Sorber, M. Van Barel, L. De Lathauwer, Tensorlab 3.0, https://www.tensorlab.net/, Mar. 2016.

[20] J. Jakabosky, S.D. Blunt, B. Himed, "Spectral-shape optimized FM noise radar for pulse agility," *IEEE Radar Conf.*, Philadelphia, PA, May 2016.

[21] M.B. Heintzelman, T.J. Kramer and S.D. Blunt, "Experimental evaluation of super-Gaussian-shaped random FM waveforms," *IEEE Radar Conference*, New York City, NY, Mar. 2022.

[22] S.D. Blunt *et al*., "Principles and applications of random FM radar waveform design," *IEEE Aerospace and Electronic Systems Mag.*, vol. 35, no. 10, pp. 20-28, Oct. 2020.